# Nuclear dynamical deformation induced hetero- and euchromatin positioning

Akinori Awazu
*Department of Mathematical and Life Sciences, Hiroshima University*
*and Research Center for Mathematics on Chromatin Live Dynamics, Kagami-yama 1-3-1, Higashi-Hiroshima 739-8526, Japan*
(Received 11 June 2015; published 14 September 2015)

We studied the role of active deformation dynamics in cell nuclei in chromatin positioning. Model chains containing two types of regions, with high (euchromatic) or low (heterochromatic) mobility, were confined in a pulsating container simulating a nucleus showing dynamic deformations. Brownian dynamic simulations show that the positioning of low mobility regions changes from sites near the periphery to the center if the affinity between these regions and the container periphery disappears. The former and latter positionings are similar to the "conventional" and "inverted" chromatin positionings in nuclei of normal differentiated cells and cells lacking Lamin-related proteins. Additionally, nuclear dynamical deformation played essential roles in "inverted" chromatin positioning.

DOI: 10.1103/PhysRevE.92.032709 PACS number(s): 87.16.Sr, 87.15.nr, 87.16.Zg

The structure and dynamics of interphase chromosomes have been recognized to play important roles in several activities in eukaryotes such as gene regulation and cell differentiation [1–12]. Recently, several mesoscopic theoretical and simulation models of chromosomes were proposed to investigate mechanisms underlying the formation of several features of intranuclear architecture, such as the chromosome territories, transcription factories, topologically associating domains, conventional, and inverted positioning of heterochromatin [13–23].

The cell nuclei are reportedly involved in several aspects of intracellular dynamics, such as oscillation, rotation, and deformation driven by the oscillatory dynamics of the cytoskeleton, including microtubule and actin networks [24–37]. The dynamics of nuclei often affect the positioning and structures of intranuclear architectures and gene expression via interactions between the chromosomes and the nuclear periphery [24–35,37–41]. Moreover, the membrane proteins such as lamin $A$, $B$, $C$, and lamin receptors anchor heterochromatin to the nuclear periphery [10,11,42–47]. Thus, the influence of nuclear dynamics and the physicochemical aspects of the nuclear membrane on chromosome conformations must be elucidated to clarify the activities involved in the intranuclear processes and their mechanisms. However, only few theoretical studies have focused on such issues.

Here, we introduce a simplified chromosome model that consists of $M$ chains with two types of regions, one with high mobility and the other with low mobility, in a 3D spherical pulsating container. The regions with high and low mobility are regarded as eu- and heterochromatic regions, respectively; heterochromatic regions consist of densely compacted DNA and proteins to silence transcription and hence experience larger viscous drag than euchromatic regions. Pulsation of the container, which is generated by temporal variations of the container's radius, simulates the deformation of nuclei [Fig. 1(a)]. Thus, by focusing on the deformation-dependent behaviors of this model, we clarify the possible contributions of nuclear dynamics to chromatin positioning.

In this model, each chain is constructed by $N$ spherical particles with diameter $d$ and are connected by a spring with natural length $d$. The motion of each particle is given as Brownian motion with each drug coefficient. The motion of each particle obeys

$$\gamma_i \dot{\mathbf{x}}_\mathbf{i} = -\nabla_i (V_{\rm int}(\{\mathbf{x}_i\}) + V_{\rm con}(\{\mathbf{x}_i\})) + \eta_i(t), \tag{1}$$

$$\langle \eta_i(t)\eta_i(t')\rangle = 2\gamma_i G\delta(t-t'), \tag{2}$$

where $\mathbf{x}_i$ and $\gamma_i$ are the position and drug coefficient of the $i$th particle, respectively, and $\eta_i$ and $G$ are the random force (Gaussian white noise) working on the $i$th particle and its magnitude, respectively. Here, $\gamma_i = \gamma_H$ for high mobility particles ($H$ particles) and $\gamma_i = \gamma_L$ for low mobility particles ($L$ particles).

The interaction potential between particles is expressed by $V_{\rm int}(\{\mathbf{x}_i\}) = V^{ch}(\{\mathbf{x}_i\}) + V^{sf}(\{\mathbf{x}_i\})$, where the former represents the elastic potential between two connected particles and is given by

$$V^{ch} = \sum_i \frac{k_c}{2}(|\mathbf{x}_i - \mathbf{x}_{i+1}| - d)^2, \tag{3}$$

and the latter represents the soft core repulsive potential due to the excluded volume between two particles; this is given by

$$V^{sf} = \sum_{i<j} \begin{cases} \frac{k_e}{2}(|\mathbf{x}_i - \mathbf{x}_j| - d)^2 & (|\mathbf{x}_i - \mathbf{x}_j| < d), \\ 0 \quad \text{(otherwise)} \end{cases} \tag{4}$$

with $k_e$ and $k_c$ as constants.

The motion of particle is restricted by the container; soft-core repulsion exists between the container wall and all particles, whereas short-range attraction exists between the wall and $L$ particles. Short-range attraction arises from the interactions between the nuclear periphery and heterochromatic regions through Lamin-related proteins. Thus, the potential is given as $V_{\rm con}(\{\mathbf{x}_i\}, R) = \sum_i V^i_{\rm wall}(\mathbf{x}_i, R) + \sum_{\gamma_i=\gamma_L} V^i_{\rm lamin}(\mathbf{x}_i, R)$, where

$$V^i_{\rm wall}(\mathbf{x}_i, R) = \begin{cases} \frac{k_w}{2}\left[|\mathbf{x}_i| - \left(R - \frac{d}{2}\right)\right]^2 & \left(|\mathbf{x}_i| > R - \frac{d}{2}\right), \\ 0 \quad \text{(otherwise)}, \end{cases} \tag{5}$$

$$V^i_{\rm lamin}(\mathbf{x}_i, R) = \begin{cases} -k_l|\mathbf{x}_i| & (|\mathbf{x}_i| > R - d), \\ 0 \quad \text{(otherwise)} \end{cases} \tag{6}$$

with constants $k_w$, $k_l$ and the container radius $R$ [48].

 

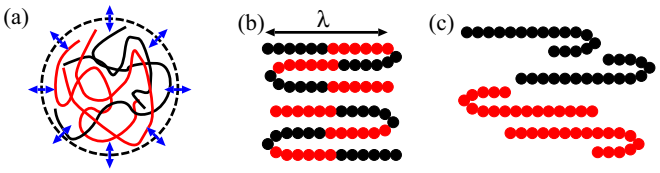


FIG. 1. (Color online) Illustrations of (a) confined chains in pulsating container, and (b) $H$-$L$ mixed chains and (c) $H$ chains and $L$ chains consisting of $H$ particles [grey (red)] and $L$ particles (black).

We assume that the container pulsates periodically according to the temporally periodic variations of its radius as

$$R = R_o + A \sin \omega t, \tag{7}$$

where $R_o$, $A$, and $\omega$ are the basic radius, amplitude, and frequency of pulsations, respectively. The deformation of nuclei in cells is not periodic, but using this model, we can clarify the characteristics and mechanisms of the contributions of nuclear deformable motion to chromosome positioning. Additionally, we achieved the same qualitative results as obtained if $R$ exhibits random walk in a harmonic potential field $\frac{1}{2}k_r(R - R_o)^2$ with constant $k_r$.

We focused on the segregation patterns of $H$ and $L$ particles when the following chains were confined in the container: (i) $H$-$L$ mixed chains: each chain consists of $H$- and $L$-particle regions connected periodically, where the length of each $H$- and $L$-particle region along the center is $\lambda/2$ [see Fig. 1(b)]; and (ii) $H$ chains and $L$ chains: half of all chains consist of only the $H$-particle region and the other half consist of only the $L$-particle region [see Fig. 1(c)]. In the case of a large $N$, $H$-$L$ mixed chains provide simple models of chromosomes containing eu- and heterochromatic regions, and $H$ chains and $L$ chains provide simple models of the euchromatin-rich and heterochromatin-rich chromosomes, respectively.

Here, we considered the following parameters: $\gamma_H = 1$, $\gamma_L = 10$, $k_e = k_c = k_w = 1024$, $G = 1$, and $d = 1$. In recent experimental observations, the volume fraction of macromolecules in the nucleus is estimated as $0.2 \sim 0.3$ [22]. Thus we focused on the case of $(d/2)^3 MN/R_o^3 \sim 0.296$ ($MN = 512$ and $R_o = 6.0d$). We confirmed that the qualitative aspects of the system as shown below, are not sensitive for $NM$ and $R_o$ if the volume fraction of particles is similar. For example we obtained similar results in the case of $MN = 1024$ and $R_o = 7.5d$ with $(d/2)^3 MN/R_o^3 \sim 0.30$. Unfortunately, the ratio of $\gamma_H$ to $\gamma_L$ is unclear experimentally. However, we can obtain qualitatively similar results if $\gamma_L$ is larger enough than $\gamma_H$.

First, we focused on the segregation pattern of $H$-$L$ mixed chains in the pulsating container. Figure 2 shows typical snapshots of the $H$- and $L$-particle distribution in two-dimensional (2D) cross sections in 3D space (particles at $-d/2 \leqslant x \leqslant d/2$, $-d/2 \leqslant y \leqslant d/2$, and $-d/2 \leqslant z \leqslant d/2$ on the $x - y - z$ 3D space are shown) for $M = 1$, $N = 512$, $\lambda = 64d$, $\omega = 4$, and $A = d/4$ with (a) $k_l = 10$, (b) $k_l = 0$. More $H$ particles ($L$ particles) tend to distribute near the center (periphery) of the container than $H$ particles ($L$ particles) for $k_l = 10$, while an opposite distribution occurs for $k_l = 0$. These trends in positioning of $H$ and $L$ particles are similar to the "conventional" and "inverted" eu- and heterochromatin positioning, respectively, observed in nuclei of normal differentiated cells and cells lacking lamin-related proteins, such as mouse rod photoreceptor cells [10,11].

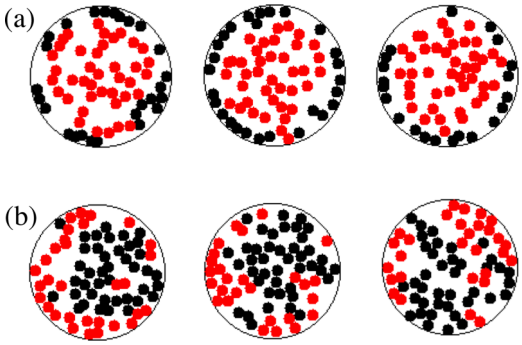


FIG. 2. (Color online) Typical snapshots of the distribution of $H$ particles [grey (red)] and $L$ particles (black) of $H$-$L$ mixed chains ($M = 1$, $N = 512$, $\lambda = 64d$) on $x \sim 0$ (left), $y \sim 0$ (center), and $z \sim 0$ (right) 2D cross sections on $x - y - z$ 3D space. (a) $k_l = 10$, (b) $k_l = 0$, with $\omega = 4$ and $A = d/4$.

It is easily understood that the affinity between the container periphery and $L$ particles contribute considerably to the former segregation patterns. On the other hand, if the container does not pulsate, the distributions of $H$ and $L$ particles become uniform when $k_l = 0$ because such situations are equivalent to thermodynamic equilibrium, thus indicating that the latter segregation pattern is the result of the pulsations of the container.

To observe the contributions of the pulsations of the container to pattern formations of $H$-$L$ mixed chains, we focused on the pulsating frequency dependency of $H$- and $L$-particle distributions for $k_l = 0$. Figure 3 shows the relative radial distributions $P(r)$ for some $\omega$ in the cases of (a) $M = 1$, $N = 512$, and $\lambda = 64d$, and (b) $M = 4$, $N = 128$, and $\lambda = 64d$. Here, $P(r) = P_L(r) - P_H(r)$, where $P_m(r) = n_m(r)/4\pi r^2$ ($m = H$ or $L$) are the respective radial particle distributions, $r$ is the distance from the origin, and $n_m(r)$ is the frequency of $m$ particles in the region between $r$ and $r + dr$ for $dr = 0.1$. Here, $P(r) = 0$ always holds when $\omega = 0$ (except for small errors due to the finite run time and sample number of simulations). The figures indicate the appropriate values of $\omega$ for the segregation of the $H$ and $L$ particles. We obtained similar results for $\lambda = 32d$ and $\lambda = 128d$.

Similar results were obtained for $H$ chains and $L$ chains confined in the pulsating container. Figures 4(a)–4(c) show

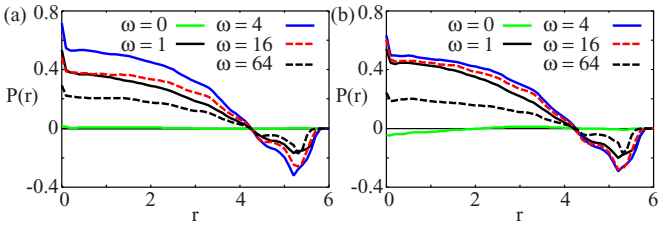


FIG. 3. (Color online) $P(r)$ of $H$-$L$ mixed chains for $\omega = 0,1,4,16,64$ in the cases of (a) $M = 1$, $N = 512$, and $\lambda = 64d$, and (b) $M = 4$, $N = 128$, and $\lambda = 64d$ with $k_l = 0$.

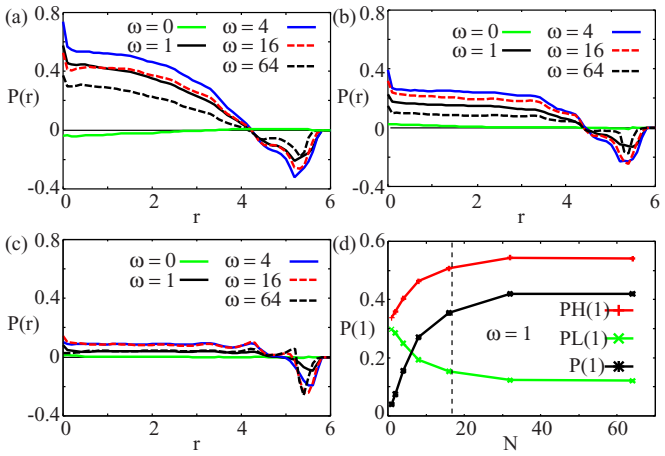


FIG. 4. (Color online) $P(r)$ of the system consists of $H$ chains and $L$ chains for $\omega = 0,1,4,16,64$ in the cases of (a) $M = 8$, $N = 64$, (b) $M = 128$, $N = 4$, and (c) $M = 512$, $N = 1$ with $k_l = 0$. (d) $P_H(1)$, $P_L(1)$, and $P(d)$ as function of $N$ for $NM = 512$ and $\omega = 1$ with $k_l = 0$ where dot curve indicates $N = 5.5^{5/3}$.

the relative radial distributions $P(r)$ for some $\omega$ in the cases of (a) $M = 8$ and $N = 64$, (b) $M = 128$ and $N = 4$, and (c) $M = 512$ and $N = 1$ with $k_l = 0$. The distribution of the $H$ and $L$ particles exhibits $\omega$ dependency similar to that of $H$-$L$ mixed chains. However, the segregation strength becomes weak with the decrease in $N$. For example $P(d)$ that gives a typical $P(r)$ in the bulk of the container decreases drastically with the decrease in $N$ if $(dN)^{3/5}$ is smaller than $\sim(R_o - d/2)$ ($N$ is smaller than $\sim(R_o - d/2)^{5/3}/d = 5.5^{5/3}$) as shown in Fig. 4(d).

The mechanisms underlying the pulsation-induced segregation pattern can be explained as follows. It is noted that $H$ and $L$ particles are equally compressed when the container contracts. On the other hand, after the expansion of the container, $H$ particles positioned at the outer region of particle accumulations diffuse closer to the periphery of the container faster than $L$ particles. Therefore, by iterating the contractions and expansions of the container, the region near the container periphery tends to be occupied by more $H$ particles than $L$ particles.

Now, we consider the case where $H$ particles construct long chains such that the average distance between two edges $\sim (dN)^{3/5}$ (estimated by the arguments of self-avoiding random walk [49]) is longer than $(R_o - d/2)$, or where each $H$-$L$ mixed chain involves $H$-particle regions as long as $(\lambda/2)^{3/5} > (R_o - d/2)$. In such cases, $H$ particles near the center are pulled by those migrating near the periphery since they often belong to the same chain or the same region. Thus, most of the $H$ particles accumulate gradually near the periphery of the container.

On the other hand, when the particles move individually or form only short chains, the influence of the pulsations on particles in the bulk of the container is negligibly weak because the amplitude of the pulsations is not as large as mentioned below. Thus, the segregation occurs only near the periphery of the container in such cases.

Notably, we found that $L$ particles tend to accumulate in the central region of the container in such smaller $A = d/4$ than $R_o = 6d$ for $k_l = 0$. We also confirm qualitatively the same properties of $P(r)$ in the case of $A = d/8$ although typical values of $P(d)$ become small. Thus, such segregation does not need pulsations with large amplitudes. This fact indicates that weak, but not zero, active deformation of the nucleus is enough for the inverted chromatin positioning in cells without Lamin-related proteins.

Finally, we evaluated the relationships between the parameter sets employed in the present simulations and those in experimental situations. The characteristic spatial and temporal scale of the present model is given as follows: (i) the number of particles, which indicates the basic units of the model chromosome chain confined in the container, is $\sim 10^3$; (ii) the diameter of the container (model nucleus) is $\sim 10$ times the diameter of a single particle; (iii) $\tau_{\rm diff}$, which gives the diffusion time scale of particles in the space with the length scale $A$ ($=d/8 \sim d/4$, $d = 1$) when particles do not construct chains, is given by $\sim A^2/(G/\gamma_H) \sim 10^{-2\sim-1}$; and (iv) $\tau_{\rm nuc}$, which gives the time scale of the deformation of a container with the length scale $A$, is given by $\sim\omega^{-1} \sim 10^{-2\sim0}$. Here, $\tau_{\rm nuc}/\tau_{\rm diff}$ is given as $10^{-1} \sim 10^2$.

It is noted that chromosomes have long range correlated chromatin domains named "topologically associated domains" (TADs) which are formed by the association of the local chromatin fibers with some megabase pairs [50–52]. Thus, to avoid the considerations of complex spatial structures of TADs, we assume a basic unit constructing chromosomes as a $\sim 10^7$-bp chromatin containing some TADs. The nucleus of the mammalian cell contains $\sim 10^{10}$ bp, indicating that $\sim 10^3$ basic units of chromosomes are confined in each nucleus. Moreover, the average diameter of each basic unit of chromosome, $d_b$, is roughly estimated as $\sim\sqrt{10^7} \times 3.4$ Å $\sim 10^{-6}$ m. The diameter of the nucleus of mammalian cells is estimated as $\sim 10^{-5}$ m, indicating a nuclear diameter of $\sim 10 d_b$ m. These relations are similar to those in the present simulations [(i) and (ii)].

The drag coefficient $\gamma$ for each basic unit of chromosome is estimated as $=6\pi\eta(d_b/2) \sim 10^{-9}$ kg s$^{-1}$, where $\eta \sim 10^{-4}$ kg m$^{-1}$ s$^{-1}$ represents the viscosity of water. $G$ is not equal to $k_BT$ because the intranuclear environment is in a state of thermodynamic nonequilibrium owing to the energy flow via the interactions between chromosomes and several proteins; however, in this model we assume the order of $G$ is similar to $k_BT$. Here, $k_B \sim 10^{-23}$ m$^2$ kg s$^{-2}$ K is the Boltzmann constant and $T = 300$ K. Then, $G/\gamma \sim 10^{-12}$ m$^2$ s$^{-1}$. In recent experiments, the distance between the center and a part of the periphery of the nucleus varies as $\sim 10^{-7}$ m ($\sim 10^{-1} d_b$ m) per $\sim 10^0$ s [35]. Thus, $\tau_{\rm diff} \sim (10^{-7}\ {\rm m})^2/(10^{-12}\ {\rm m}^2\ {\rm s}^{-1}) \sim 10^{-2}$ s, $\tau_{\rm nuc} \sim 10^0$ s, and $\tau_{\rm nuc}/\tau_{\rm diff} \sim 10^2$ are obtained.

The above estimations indicate that the ratios of the characteristic time scale of the diffusion of chromosomes to that of the deformation of nucleus in both the present and experimental situations are similar. Thus, the present simulation results can be applied to study and understand the intranuclear pattern formations of chromosomes in experimental situations.

In this study, we focused on the behaviors of chains containing high and low mobility regions that were confined in a pulsating container to understand the contributions of nuclear active deformation dynamics to the intranuclear positioning of hetero- and euchromatin. We found that the positioning of

low mobility regions (which corresponded to heterochromatic regions) transitions from sites near the periphery to the central region of the container if the affinity between these regions and the container periphery disappears. The former and latter positionings are similar to the "conventional" and "inverted" chromatin positionings observed in the nuclei of normal differentiated cells and cells lacking lamin-related proteins, such as mouse rod photoreceptor cells.

Recently, some theoretical models of the transition between "conventional" and "inverted" heterochromatin positioning were proposed [21–23]. These models tried to explain the mechanism of such transitions using certain assumptions (some of which could not be verified experimentally), such as the differences of chromatin-chromatin binding affinities among hetero-hetero, hetero-eu, and eu-euchromatins, the difference of the characteristic length of hetero- and euchromatic regions in chromosomes. Such inhomogeneity of intrachromosome properties may play important roles to determine the intranuclear chromatin positioning; however, the present results indicate that active nuclear deformation, which has been previously observed in several cells, drives "inverted" heterochromatin positioning without specific interactions among chromatins. Thus, we propose that the active nuclear deformations contribute considerably to the determination of intranuclear chromosome architectures in addition to the previously proposed interchromatin interactions.

However, the present model does not sufficiently describe the transient behaviors observed in experiments. For example, some middle scale heterochromatin domains were observed transiently before the final "inverted" chromatin positioning with only one large heterochromatin domain in experiments [10,11], which may be difficult for the present model to reproduce. Now, we progress the modifications of the model to describe the entire processes of the formation of intranuclear chromosome architectures.

From the point of view of polymer physics, the presented models are simple block-co-polymer populations or polymer mixtures with different mobilities confined in a small space under nonequilibrium boundary conditions. We provided a brief analysis to explain the present simulation results. However, further detailed studies based polymer dynamics may explain the present simulation results more precisely. More detailed theoretical studies on the presented segregation pattern formation are important for the fields of soft matter and statistical physics.

The author is grateful to H. Ochiai, S. Lee, S. Tashiro, and H. Nishimori for their fruitful discussion. This research was supported in part by the Platform Project for Supporting in Drug Discovery and Life Science Research (Platform for Dynamic Approaches to Living System) from the Ministry of Education, Culture, Sports, Science (MEXT) and the Japan Agency for Medical Research and Development (AMED), and the Grant-in-Aid for Scientific Research on Innovative Areas "Spying minority in biological phenomena" (No. 3306) (Grant No. 24115515) and "Initiative for High-Dimensional Data-Driven Science through Deepening of Sparse Modeling" (No. 4503) (Grant No. 26120525) of MEXT of Japan.

[1] T. Cremer and C. Cremer, Nat. Rev. Genet. **2**, 292 (2001).
[2] L. A. Parada and T. Misteli, Trends Cell Biol. **12**, 425 (2002).
[3] C. S. Osborne, L. Chakalova, K. E. Brown, D. Carter, A. Horton, E. Debrand, B. Goyenechea, J. A. Mitchell, S. Lopes, W. Reik *et al.*, Nat. Genet. **36**, 1065 (2004).
[4] S. T. Kosak and M. Groudine, Genes Dev. **18**, 1371 (2004).
[5] T. Takizawa, K. Meaburn, and T. Misteli, Cell **135**, 9 (2008).
[6] P. Meister, B. D. Towbin, B. L. Pike, A. Ponti, and S. M. Gasser, Genes Dev. **24**, 766 (2010).
[7] T. Cremer and M. Cremer, Cold Spring Harb. Perspect. Biol. **2**, a003889 (2010).
[8] P. K. Geyer, M. W. Vitalini, and L. L. Wallrath, Curr. Opin. Cell Biol. **23**, 354 (2011).
[9] W. A. Bickmore, Annu. Rev. Genomics Hum. Genet. **14**, 67 (2013).
[10] I. Solovei, M. Kreysing, C. Lanctot, S. Kosem, L. Peichl, T. Cremer, J. Guck, and B. Joffe, Cell **137**, 356 (2009).
[11] I. Solovei, A. S. Wang, K. Thanisch, C. S. Schmidt, S. Krebs, M. Zwerger, T. V. Cohen, D. Devys, R. Foisner, L. Peichl *et al.*, Cell **152**, 584 (2013).
[12] A. Bolzer, G. Kreth, I. Solovei, D. Koehler, K. Saracoglu, C. Fauth, S. Muller, R. Eils, C. Cremer, M. Speicher *et al.*, PLoS Biol. **3**, e157 (2005).
[13] M. Bohn and D. W. Heermann, PLoS One **5**, e12218 (2010).
[14] K. Finan, P. R. Cook, and D. Marenduzzo, Chromosome Res. **19**, 53 (2011).
[15] M. Barbieri, M. Chotalia, J. Fraser, L. M. Lavitas, J. Dostie, A. Pombo, and M. Nicodemi, Proc. Natl. Acad. Sci. USA **109**, 16173 (2012).
[16] H. Jerabek and D. W. Heermann, PLoS One **7**, e37525 (2012).
[17] M. D. Stefano, A. Rosa, V. Belcastro, D. di Bernardo, and C. Micheletti, PLoS Comput. Biol. **9**, e1003019 (2013).
[18] C. A. Brackley, S. Taylor, A. Papantonis, P. E. Cook, and D. Marenduzzo, Proc. Natl. Acad. Sci. USA **110**, E3605 (2013).
[19] A. Rosa and R. Everaers, Phys. Rev. Lett. **112**, 118302 (2014).
[20] D. Jost, P. Carrivain, G. Cavalli, and C. Vaillant, Nucleic Acids Res. **42**, 9553 (2014).
[21] N. Ganai, S. Sengupta, and G. I. Menon, Nucleic Acids Res. **42**, 4145 (2014).
[22] H. Jerabek and D. W. Heermann, Int. Rev. Cell. Mol. Biol. **307**, 351381 (2014).
[23] A. Awazu, Phys. Rev. E **90**, 042308 (2014).
[24] C. M. Pomert, Exp. Cell Res. **5**, 191 (1953).
[25] K. T. S. Yao and D. J. Ellingson, Exp. Cell Res. **55**, 39 (1969).
[26] P. C. Park and U. De Boni, Exp. Cell Res. **197**, 213 (1991).
[27] H. Masuda, R. Miyamoto, T. Haraguchi, and Y. Hiraoka, Genes Cells **11**, 337 (2006).
[28] K. N. Dahl, A. J. Ribeiro, and J. Lammerding, Circ. Res. **102**, 1307 (2008).
[29] A. C. Rowat, J. Lammerding, and J. H. Ipsen, Biophys. J. **91**, 4649 (2006).
[30] A. Brandt, F. Papagiannouli, J. Grosshans *et al.*, Curr. Biol. **16**, 543 (2006).

[31] A. Kumar and G. V. Shivashankar, PLoS ONE **7**, e33089 (2012).
[32] D. Bhattacharya, S. Talwar, G. V. Shivashankar *et al.*, Biophys. J. **96**, 3832 (2009).
[33] J. D. Pajerowski, K. N. Dahl, D. E. Discher *et al.*, Proc. Natl. Acad. Sci. USA **104**, 15619 (2007).
[34] G. V. Shivashankar, Annu. Rev. Biophys. **40**, 361 (2011).
[35] S. Talwar, A. Kumar, M. Rao, G. I. Menon, and G. V. Shivashankar, Biophys. J. **104**, 553 (2013).
[36] K.-D. Kim *et al.*, J. Cell Sci. **126**, 5271 (2013).
[37] N. M. Ramdas and G. V. Shivashankar, J. Mol. Bio. **427**, 695 (2015).
[38] C. H. Thomas, J. H. Collier, C. S. Sfeir, and K. E. Healy, Proc. Natl. Acad. Sci. USA **99**, 1972 (2002).
[39] K. J. Chalut *et al.*, Biophys. J. **103**, 2060 (2012).
[40] A. Barascu *et al.*, Nucleus **3**, 411 (2012).
[41] G. Fabrikant, S. Gupta, G. V. Shivashankar, and M. M. Kozlov, Biophys. J. **105**, 1316 (2013).
[42] N. Zuleger, M. I. Robson, and E. C. Schirmer, Nucleus **2**, 339 (2011).
[43] L. E. Finlan, D. Sproul, I. Thomson, S. Boyle, E. Kerr, P. Perry, B. Ylstra, J. R. Chubb, and W. A. Bickmore, PLoS Genet. **4**, e1000039 (2008).
[44] J. M. Zullo, I. A. Demarco, R. Pique-Regi, D. J. Gaffney, C. B. Epstein, C. J. Spooner, T. R. Luperchio, B. E. Bernstein, J. K. Pritchard, K. L. Reddy *et al.*, Cell **149**, 1474 (2012).
[45] K. Van Bortle and V. G. Corces, Cell **152**, 1213 (2013).
[46] N. Zuleger, S. Boyle, D. A. Kelly, J. I. de las Heras, V. Lazou, N. Korfali, D. G. Batrakou, K. N. Randles, G. E. Morris, D. J. Harrison *et al.*, Genome Biol. **14**, R14 (2013).
[47] D. Camozzi *et al.*, Nucleus **5**, 427 (2014).
[48] If $V^{sf}$ and $V^{i}_{\text{wall}}$ are given by the repulsive Lenard-Jones potential, or $V^{ch}$ is given by the combination of the finitely extensible nonlinear elastic (FENE) potential and Lenard-Jones potential, the results are qualitatively unchanged.
[49] P.-G. de Gennes, *Scaling Concepts in Polymer Physics* (Cornell University Press, London, 1979).
[50] J. R. Dixon *et al.*, Nature (London) **485**, 376 (2012).
[51] E. Nora *et al.*, Nature (London) **485**, 381 (2012).
[52] G. Cavalli and T. Misteli, Nat. Struct. Mol. Biol. **20**, 290 (2013).